draw the conclusion that the NO_2 flux close to the shuttle tiles is considerably enhanced over that near the bulkhead. Assuming that the conditions for the two flights are the same (mass spectrometer data from flight 41-B and glow data from flight 41-D), and that the glow intensity of the shuttle tiles is the same as that of Si-coated Z302, we deduce that $\Phi(NO_2^*)/\Phi(NO_2) \simeq 0.01$-$0.1$. Thus the mass spectrometer data indicate that NO_2 desorbed from the surface is present in sufficient amount to further consider NO_2 a viable candidate for causing the glow.

To pursue this analysis, let us assume that NO is present on the surfaces of the space shuttle (from the ambient, from surface reaction between N and O (ref. 16), from chemical reaction of fast O with the shuttle materials, or from contamination caused by attitude thruster firings[8]), and that O atoms striking the surface recombine with the adsorbed NO to yield NO_2^*:

$$\text{NO (adsorbed)} + \text{O (fast)} \rightarrow NO_2^* \text{ (fast)} \quad (1)$$

This is an example of the Eley-Rideal mechanism in catalysis (see ref. 17 for a discussion of this and the Langmuir-Hinshelwood mechanism). In this mechanism, the desorbed molecule is expected to carry the evolved heat of the reaction as rotational, vibrational, electronic or kinetic energy (or a mix of all these). A summary of work relevant to the shuttle glow problem is given in ref. 18. For the case under discussion, reaction (1), the excess energy is enormous: kinetic energy of O (4.5 eV, corresponding to a velocity of $7.3\ \text{km s}^{-1}$) + D_O(NO-O) (3.1 eV), or a total of 7.6 eV. The short wavelength cutoff of the glow is ~430 nm (ref. 7), corresponding to 2.9 eV in the form of electronic excitation. If the desorbed NO_2^* has a kinetic energy of 1.5 eV, as has been suggested[13], then the remainder (3.2 eV, or ~40% of the excess energy) must be partitioned between vibrational/rotational excitation of NO_2 and surface deposition of the excess energy. Results from beam experiments[18] and theoretical calculations[19] indicate that the amount of energy deposited into the surface is quite small. For example, in a theoretical study of the reaction of O with adsorbed carbon on platinum at 0 and 500 K, it was found that >90% of the energy released in the reaction appears in the product, CO. If the case of $O + NO_{ads}$ is analogous, then most of the remaining energy would appear in vibrational/rotational excitation of NO_2 (~2.8 eV); ~5% of the excess energy would be deposited in the surface (~0.4 eV). The implication of this argument is that the glow emitted by NO_2 may be more intense in the infrared than in the visible. The problem becomes even more serious if the velocity of the desorbed NO_2^* is less than that used above. In any case, the prediction from this mechanism is that the rate of desorption of NO_2 will increase with increasing [O], until a plateau is reached.

Another model is provided by the Langmuir-Hinshelwood mechanism, whereby fast O atoms are thermalized on the surface and then react with adsorbed NO to form NO_2:

$$\text{NO (adsorbed)} + \text{O (adsorbed)} \rightarrow NO_2 \text{ or } NO_2^* \quad (2)$$

Again, the NO_2 or NO_2^* would be expected to contain the excess energy, which is now considerably smaller than in the Eley-Rideal mechanism, namely only D_O^0(NO-O), 3.1 eV. Since the short-wavelength threshold is ~430 nm (2.9 eV), the remainder, 0.2 eV, is kinetic energy; this corresponds to a velocity of $0.9\ \text{km s}^{-1}$ for the desorbed NO_2. If we again use a radiative lifetime of 80 μs, then the e-folding distance becomes ~7 cm, which is not far from the observed distance. If both NO and O are strongly adsorbed on the surface and if the adsorption energies are comparable, then the rate of reaction (2), and therefore the glow intensity, will go through a maximum as [O] is increased. If, on the other hand, both NO and O are weakly bound to the surface, then the reaction will be second-order in [O] (ref. 17). We cannot yet choose between the two mechanisms, although the Langmuir-Hinshelwood mechanism seems easier to reconcile with the observations. Finally, the energies and lifetimes used above represent most probable values. In reality, there will be a distribution (perhaps maxwellian) of interaction energies, which will in turn, lead to a distribution of excitation energies in the products. For the qualitative nature of this discussion, however, it is sufficient to consider the most probable values.

The question of the origin of the surface NO merits some discussion. The four sources mentioned above are all possible, and all can provide the required [NO]. We note that, for example, semi-empirical models of the thermosphere[20] predict ambient densities [O] and [N] of $5.3 \times 10^8\ \text{cm}^{-3}$ and $6.5 \times 10^5\ \text{cm}^{-3}$, respectively, during our observational period. Hence, fluxes of ambient species onto the cabin bulkhead have been $\phi(O) = 3.4 \times 10^{14}\ \text{cm}^{-2}\ \text{s}^{-1}$ and $\Phi(N) = 4.1 \times 10^{11}\ \text{cm}^{-2}\ \text{s}^{-1}$. $\Phi(N)$ seems only just able to balance $\phi(NO_2)_b$. However, due to local-time and latitudinal/seasonal variations in the global N distribution, $\phi(N)$ went through a local minimum at the location and time of our observation and the orbital average of $\phi(N)$ is considerably higher.

The data reported here are consistent with a glow hypothesis based on NO_2 emission. However, they do not prove this hypothesis, and a number of questions remain, concerning NO_2 as the source of the radiation.

We thank E. Wulf for support and I. Kofsky for helpful comments. This work was supported by the German Bundesministerium für Forschung und Technologie under grant 01 QV 239.

Received 29 October 1985; accepted 4 March 1986.

1. *Aviat. Week Space Tech.* **116,** 19, 14 (1982).
2. Yee, J. H. & Abreu, V. *J. Geophys. Res. Lett.* **10,** 126-129 (1983).
3. Slanger, T. G. *Geophys. Res. Lett.* **10,** 130-132 (1983).
4. Papadopoulos, K. *Radio Sci.* **19,** 571-577 (1984).
5. Green, B. D. *Geophys. Res. Lett.* **11,** 576-579 (1984).
6. Prince, R. H. *Geophys. Res. Lett.* **12,** 453-456 (1985).
7. Swenson, G. R., Mende, S. B. & Clifton, K. S. *Geophys. Res. Lett.* **12,** 97-100 (1985).
8. Wulf, E. & von Zahn, U. *J. geophys. Res.* **91,** 3270-3278 (1986).
9. Stephan, K., Helm, H., Kim, Y. B., Seykora, G., Ramler, J. & Grössl, M. *J. chem. Phys.* **73,** 303-308 (1980).
10. Märk, T. D. & Hille, E. *J. chem. Phys.* **69,** 2492-2496 (1978).
11. Yee, J. H. & Dalgarno, A. in *Proc. AIAA Meet. Shuttle Environment and Operations,* Washington (1982).
12. Schwartz, S. E. & Johnston, H. S. *J. chem. Phys.* **51,** 1286-1302 (1969).
13. Mende, S. B. *et al. J. Space Rock.* **23,** 189-193 (1986).
14. Korb, L. J., Morant, C. A., Calland, R. M. & Thatcher, C. S. *Bull. Am. ceram. Soc.* **60,** 1188-1193 (1981).
15. NASA Handbook, *Space Shuttle System Payload Accommodations* Vol. XIV (Rev. H, JSC-07700, 1983).
16. Engebretson, M. J. & Mauersberger, K. *J. geophys. Res.* **84,** 839-844 (1979).
17. Glasser, R. P. H. *An Introduction to Chemisorption and Catalysis by Metals* 190-197 (Oxford University Press, New York, 1985).
18. Kofsky, I. & Barrett, J. L. *Planet. Space Sci.* (in the press).
19. Tully, J. C. *J. Chem. Phys.* **73,** 6333-6342 (1980).
20. Köhnlein, W. *Planet. Space Sci.* **28,** 225-243 (1980).

Atmospheric CH_4, CO and OH from 1860 to 1985

Anne M. Thompson

Applied Research Corporation, Landover, Maryland 20785, USA

Ralph J. Cicerone

National Center for Atmospheric Research, Boulder, Colorado 80307, USA

Atmospheric methane, CO and the gaseous OH radical are interdependent: if CH_4, CO or OH is perturbed, background concentrations of the other two constituents are affected. Perturbations to OH alter photo-oxidation rates of numerous natural and anthropogenic trace gases and affect lifetimes of those species that pass from the Earth's surface to the free troposphere and stratosphere. It is now known that global atmospheric methane con-

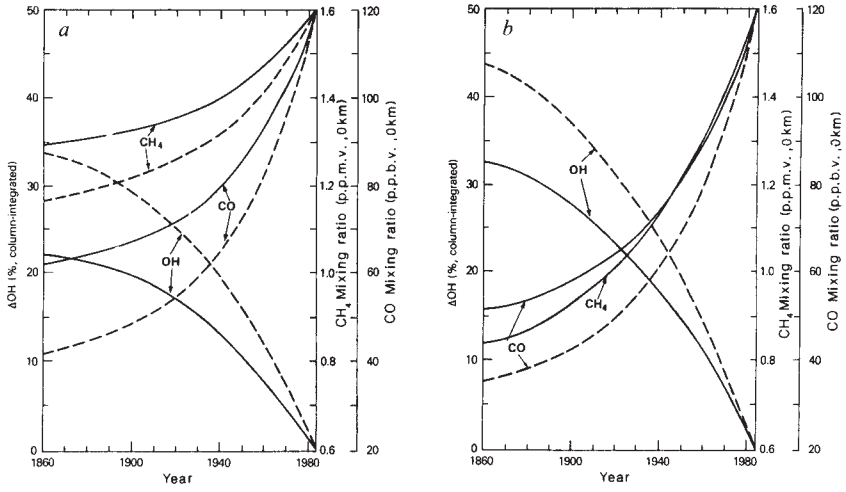

Fig. 1 Calculated ground-level methane and CO mixing ratios and per cent changes in column-integrated tropospheric OH from 1860 to 1985. Model conditions are appropriate for the mid-altitude Northern Hemisphere with low background NO_x (20–25 p.p.t.v). Calculations for low-latitude conditions (higher photolysis rates, lower O_3 and CO mixing ratios) show trends of similar magnitude, implying that the OH changes illustrated here are typical of unpolluted environments. Calculations with higher NO_x levels also show similar trends, but the magnitude of OH change is about half the increase shown here. *a*, Results from models 1 and 2 (Table 1). Methane flux is constant at all times; the calculated CH_4 increase is due solely to CO and OH changes. The solid line is from model runs with a largely anthropogenic upward flux of CO at 35% of the CO source in 1985; the dashed line assumes $flux_{CO}$ (1985) produces 65% of present-day CO. In both cases additional CO derives from CH_4 and C_2H_6 oxidation by OH and from an explicit source, S_S, representing non-methane hydrocarbon oxidation. $flux_{CO}$ and S_S vary in time as described in Table 1. *b*, Results from models 3 and 4 (Table 1). Fixed CH_4 mixing ratios follow ref. 13. Solid and broken lines as in *a*.

centrations are increasing[1–6]; less definite data suggest that carbon monoxide is also increasing[1,7–9]. Even before the measurements of refs 1–9 were made, modelling studies of CH_4–CO–OH coupling had led to predictions[10–12] of future temporal increases of CH_4 and CO. Here we look backwards in time, using a photochemical model to simulate the trace-gas composition of the unpolluted troposphere at the start of the industrial era (taken as 1860), and at intervals up to 1985. We find that the OH concentration in the background troposphere has decreased significantly and O_3 has increased due to increases of CH_4 and CO; calculated changes depend on temporal trends of NO_x ($NO_x = NO + NO_2$), for which no historical data are available. The calculations allow recent trace-gas trends affecting background chemistry and climate to be viewed in a longer-term context.

In modelling the photochemistry of the pre-industrial atmosphere it is essential to specify past concentrations of NO_x and the more stable species CH_4, CO and O_3. Before ~1960, few ambient measurements were made of these trace species, so the input to our model is based on current mixing ratios or source flux estimates extrapolated backwards in time. A summary of key species follows.

CH_4 and CO. We take two extreme methane cases: one with a minimum difference in CH_4 mixing ratio between 1860 and 1985 and one with a maximum difference. Similarly, we assume minimum and maximum temporal changes in CO and combine alternate sets of CH_4 and CO constraints to obtain four model types (Table 1). Models 1 and 2 assume a uniform CH_4 flux (constant sources) at all times, yielding 1.2–1.3 p.p.m.v. (parts per 10^6 by volume) in 1860 and 1.60 p.p.m.v. in 1985 in the models. Models 3 and 4 are based on the assumption that large differences between modern CH_4 and that extracted from ice cores[13–15] represent real changes in atmospheric composition over the past hundred years, rather than diffusive losses of trapped gases[5]. This is consistent with recently published spectroscopic measurements of past CH_4 (ref. 6). Thus, in models 3 and 4, CH_4 is present at a concentration of only 0.82 p.p.m.v. at ground level in 1860.

Choosing model input for CO is complicated because ground-level CO concentrations vary greatly, owing to the short lifetime of CO and uneven geographical distribution of CO sources[7,8]. We take 120 p.p.b.v. (parts per 10^9 by volume) CO at ground level as typical for the 1985 mid-latitude Northern Hemisphere; Southern Hemisphere CO concentrations are lower because there are fewer local sources[16,17]. Uncertainties in CO sources are treated by parameterizing two components in the model representation of the total source, $S^{total,CO}$: S_S (a surrogate for the oxidation of non-methane hydrocarbons besides C_2H_6) and $flux_{CO}$ (representing directly injected surface sources). Both S_S and $flux_{CO}$ include natural and anthropogenic contributions as described in Table 1. In ascribing 82% of present-day S_S to natural hydrocarbon sources, we follow Logan *et al.*[17], recognizing that this apportionment is still uncertain. Model runs for years before 1985 assume that natural sources contributing to S_S and $flux_{CO}$ are unchanged and anthropogenic ones scale with population or fossil-fuel usage[18]. Thus, S_S changes little in time and $flux_{CO}$ is strongly time-dependent.

Table 1 Model characteristics

Input	Model 1	Model 2	Model 3	Model 4
Past CH_4	High CH_4:constant 1985 flux		CH_4 specified from ice-core data[13]	
Past CO	Type 1-CO	Type 2-CO	Type 1-CO	Type 2-CO
Output				
1985 O_3 (0 km)	30.0 p.p.b.v.	29.8 p.p.b.v.	30.0 p.p.b.v.	29.8 p.p.b.v.
1860 O_3 (0 km)	27.7 p.p.b.v.	26.4 p.p.b.v.	25.4 p.p.b.v.	27.1 p.p.b.v.

Type 1-CO: 35% of $S^{total,CO}$ (1985) is $flux_{CO}$; type 2-CO: 65% of $S^{total,CO}$ (1985) is $flux_{CO}$. The total CO source in year t is:

$$S^{total,CO}(t) = Q_{CO}(t) + flux_{CO}(t) + S_S(t)$$

where Q_{CO}, the *in situ* photochemical formation from CH_4 and C_2H_6 oxidation, is derived from the model [$Q_{CO}(z, t)$, integrated from $z = 0$ to 15 km]; S_S (also column-integrated) explicitly represents photo-oxidation of non-methane hydrocarbons (NMHC) besides C_2H_6:

$$S_S(z, t) = S_S(z, 1985)\,[f_{NMHC,N} + r^{ff}(t) f_{NMHC,A}(1985)]$$

where $f_{NMHC,N}$ (0.82) and $f_{NMHC,A}$ (0.18 in 1985) are fractions of S_S due to oxidation of natural and anthropogenic NMHC[17]. $r^{ff}(t)$ is the ratio of fossil-fuel usage[18] in year t relative to 1985. $S_S(z, t)$ is proportional to the product of the OH number density and an exponential function with the latitude dependence of a typical OH + alkane reaction. $flux_{CO}(t)$, the model lower boundary condition for CO, signifies direct surface-injected CO sources:

$$flux_{CO}(t) = flux_{CO}(1985)\,[f_{flux,N} + r^{ff}(t) f_A^{ff}\,(1985) + r^{pop}(t) f_A^{nf}\,(1985)]$$

where $r^{pop}(t)$ is the ratio of the population in year t relative to that in 1985; f values are based on a budget[17] for Northern Hemishere CO sources; $f_{flux,N} = 0.13$ is the natural fraction of $flux_{CO}$ (oceanic flux, emissions from plants and lightning-induced wildfires); f_A^{ff} and f_A^{nf} are fossil-fuel and non-fossil-fuel (wood fuel and biomass burning) combustion components of anthropogenic $flux_{CO}$. In all models C_2H_6 at 0 km was increased from 1.0 to 1.5 p.p.b.v. between 1860 and 1985. This has negligible effect on OH and CO changes.

O_3. Ozone concentrations vary so much in time and space, even on a short timescale, that a realistic determination of tropospheric O_3 in 1860 is impossible. For simplicity we assume identical boundary conditions for O_3 in current and past-year models: these conditions are fixed stratospheric input and fixed deposition velocity[19].

H_2O, NO_x. These species and other model parameters, for example ultraviolet and visible radiation and rainout rates, are critical in determining O_3 and OH concentrations. Water vapour, radiation fluxes and rainout rates for soluble species are fixed at constant levels[19] in all model runs. Boundary conditions for odd nitrogen (NO_x) are assumed to be uniform at all times; a stratospheric odd-nitrogen source controls NO_x in the upper and mid-troposphere and a small upward flux of NO gives 20–25 p.p.t.v. (parts per 10^{12} by volume) NO_x in the boundary layer. Although NO_x sources include a large anthropogenic component that has increased during the past century, it seems reasonable to suppose that the low levels of NO_x that determine O_3 and OH in the background troposphere are supplied by non-anthropogenic sources[20,21] (for example, stratospheric injection, lightning, weak oceanic and soil fluxes of NO) which have not changed appreciably with time.

Details of the model used in the present paper and profiles of tropospheric O_3, NO_x and OH are reported in ref. 19. The model solves for a standard complement of odd O, H, N species; CO, CH_4 and species derived from CH_4 and C_2H_6 oxidation, including peroxyacetylnitrate (PAN). Simulations are performed with a steady-state model at 10–30-yr intervals. CH_4 and CO can exhibit slower transients than would be predicted from their respective 10-yr and 2-month lifetimes[11], depending on the mix of CO sources.

Figure 1 shows ground-level CH_4 and CO mixing ratios and changes in column-integrated OH (0–15 km) from 1860 to 1985. Figure 1*a* shows results assuming minimum CH_4 change between 1860 and 1985 (models 1 and 2), and Fig. 1*b* assumes maximum CH_4 change (models 3 and 4). Tropospheric OH decreases as CO and CH_4 increase, with the greatest change occurring when both CO and CH_4 undergo maximum change (model 4). In that case CH_4, CO and fractional OH increases in 1950 (relative to 1985) are similar to those presented by Levine *et al.*[22], although our NO_x level is much lower. When we calculate perturbed CH_4–CO–OH cycles at higher NO_x levels (1 p.p.b.v. at 0 km) we find that increased CH_4 and CO cause near-surface OH to increase, but total tropospheric OH decreases as in Fig. 1 (although by only half as much).

Changes in atmospheric lifetimes of hundreds of trace gases, for example, reactive hydrocarbons, sulphur and nitrogen compounds, may have occurred since 1860 as a consequence of OH perturbations. Figure 1*a* (models 1 and 2), for which no change in surface CH_4 emissions is assumed, shows that CO increases and OH decreases could have caused background-level CH_4 to increase by 24–37% from 1860 to 1985. Figure 1*b*, however, implies that CH_4 doubling since 1860 requires a change in CH_4 fluxes as well as altered background OH in response to CO changes.

Changes in CO–CH_4–OH chemistry affect climate because O_3, CH_4 and CO_2 (to which CO converts by OH oxidation) are 'greenhouse' gases. Increases in CH_4 and CO cause tropospheric ozone to increase because CH_4 and CO contribute to photochemical O_3 production[23–25]. The temporal changes shown in Fig. 1 imply an 8–18% tropospheric O_3 increase from 1860 to the present (Table 1); observations point to a recent temporal increase in tropospheric O_3 (refs 26, 27). O_3 perturbations instantaneously alter the Earth's infrared radiative forcing. If there has been sufficient time for a temperature response, this could have caused a small rise in global temperature, depending on the altitude profile of the O_3 increase[28,29]. Atmospheric CO increases affect radiation by supplying CO_2 (provided that OH remains at adequate levels), and by suppressing OH and allowing O_3 and CH_4 to accumulate, even if CH_4 emissions do not increase. For example, atmospheric CO_2 formed from the reaction OH+CO in 1860 ($8–16\times10^{10}$ molecules cm^{-2} s^{-1}, integrated through the troposphere) exceeded the direct fossil-fuel source of CO_2, that is, 2.6×10^{10} molecules cm^{-2} s^{-1} (ref. 18). Approximately 75% of this CO was natural in origin (Table 1).

A.M.T. acknowledges partial support from the NASA Tropospheric Chemistry Office. The National Center for Atmospheric Research is sponsored by NSF.

Received 25 November 1985; accepted 17 February 1986.

1. Graedel, T. E. & McRae, J. E. *Geophys. Res. Lett.* **7**, 977–979 (1980).
2. Rasmussen, R. A. & Khalil, M. A. K. *J. geophys. Res.* **86**, 9826–9832 (1981).
3. Blake, D. R. *et al. Geophys. Res. Lett.* **9**, 477–480 (1982).
4. Rasmussen, R. A. & Khalil, M. A. K. *J. geophys. Res.* **89**, 11599–11605 (1984).
5. Ehhalt, D. H., Zander, R. J. & Lamontagne, R. A. *J. geophys. Res.* **88**, 8442–8446 (1983).
6. Rinsland, C. P., Levine, J. S. & Miles, T. *Nature* **318**, 245–249 (1985).
7. Seiler, W., Giehl, H., Brunke, E. & Halliday, E. *Tellus* **36B**, 219–231 (1984).
8. Khalil, M. A. K. & Rasmussen, R. A. *Science* **224**, 54–56 (1984).
9. Rinsland, C. P. & Levine, J. S. *Nature* **318**, 250–254 (1985).
10. Chameides, W. L., Liu, S. C. & Cicerone, R. J. *J. geophys. Res.* **82**, 1795–1798 (1977).
11. Sze, N. D. *Science* **195**, 673–674 (1977).
12. Hameed, S., Pinto, J. P. & Stewart, R. W. *J. geophys. Res.* **84**, 763–768 (1979).
13. Khalil, M. A. K. & Rasmussen, R. A. *Atmos. Envir.* **19**, 397–407 (1985).
14. Stauffer, B., Fischer, G., Neftel, A. & Oeschger, H. *Science* **229**, 1386–1388 (1985).
15. Craig, H. & Chou, C. C. *Geophys. Res. Lett.* **9**, 1221–1224 (1982).
16. Seiler, W. *Tellus* **26**, 116–135 (1974).
17. Logan, J. A., Prather, M. J., Wofsy, S. C. & McElroy, M. B. *J. geophys. Res.* **86**, 7210–7254 (1981).
18. Keeling, C. D. *Tellus* **25**, 174–198 (1973).
19. Thompson, A. M. & Cicerone, R. J. *J. geophys. Res.* (submitted); **87**, 8811–8826 (1982).
20. Levy II, H., Mahlman, J. D. & Moxim, W. J. *Geophys. Res. Lett.* **7**, 441–444 (1980).
21. Liu, S. C., McFarland, M., Kley, D. & Zafiriou, O. C. *J. geophys. Res.* **88**, 1360–1368 (1983).
22. Levine, J. S., Rinsland, C. P. & Tennille, G. M. *Nature* **318**, 254–257 (1985).
23. Fishman, J., Solomon, S. & Crutzen, P. J. *Tellus* **31**, 432–446 (1979).
24. Fishman, J. & Seiler, W. *J. geophys. Res.* **88**, 3662–3670 (1983).
25. Chameides, W. L. & Walker, J. C. G. *J. geophys. Res.* **78**, 8751–8760 (1973).
26. Bojkov, R. *Spec. Envir. Rep.* no. 16 (World Meteorological Organization, Geneva, 1984).
27. Logan, J. A. *J. geophys. Res.* **90**, 10463–10482 (1985).
28. Fishman, J., Ramanathan, V., Crutzen, P. J. & Liu, S. C. *Nature* **282**, 818–820 (1979).
29. Ramanathan, V., Cicerone, R. J., Singh, H. B. & Kiehl, J. T. *J. geophys. Res.* **90**, 5547–5566 (1985).

Spreading direction in the central South China Sea

Guy Pautot*, Claude Rangin†, Anne Briais‡, Paul Tapponnier‡, Paul Beuzart*, Gilles Lericolais*, Xavier Mathieu§, Jinlong Wu‖, Shuqiao Han‖, Hengxiu Li‖, Yingxian Lu‖ & Jicheng Zhao‖

* IFREMER, Centre de Brest, BP 337, 29273 Brest Cedex, France
† Université de Paris 6, Département de Géologie Structurale, 4 Place Jussieu, 75252 Paris Cedex 05, France and Institut Français du Pétrole, l'Avenue de Bois-Préau, 92500 Rueil Malmaison, France
‡ Institut de Physique du Globe, Laboratoire de Tectonique et Mécanique de la Lithosphére, Université de Paris 6, 4 Place Jussieu, 75252 Paris Cedex 05, France
§ Université de Bretagne Occidentale, 615 "Océanologie et Géodynamique" 6, Avenue Le Gorgeu, 29283 Brest Cedex, France
‖ First Institute of Oceanography, National Bureau of Oceanography, PO Box 98, Qingdao, China

Recent work[1,2] indicates that the South China Sea is an 'Atlantic-type' marginal basin of late Tertiary age. Magnetic anomalies in the eastern part of the sea are consistent with seafloor spreading directed approximately north–south[1,2]. We present here a new morphostructural study based on coupled seabeam mapping and single-channel seismic reflection profiling, which reveals dominant normal fault scarps, striking N50° E between 113 and 119° E longitude near the axis of this basin. Such a structural fabric implies a NW–SE spreading direction, at least in the 150–200-km-wide axial region of the South China Sea, and places new constraints on geodynamic models for the formation of this basin in the tectonic and palaeogeographic framework of South-East Asia and the South-West Pacific.

The South China Sea (Nanhai), largest of the marginal basins of the western Pacific, is bounded by the continental margins